

ICAS: Detecting Training Data from Autoregressive Image Generative Models

Hongyao Yu

chrisqewx@gmail.com

Tsinghua Shenzhen International Graduate School, Tsinghua University Harbin Institute of Technology, Shenzhen, Shenzhen, Guangdong, China

Hao Fang

fang-h23@mails.tsinghua.edu.cn
Tsinghua Shenzhen International Graduate School, Tsinghua University Shenzhen, Guangdong, China

Bin Chen*

chenbin2021@hit.edu.cn
Harbin Institute of Technology, Shenzhen, Shenzhen, Guangdong, China

Yixiang Qiu

qiu-yx24@mails.tsinghua.edu.cn
Tsinghua Shenzhen International Graduate School, Tsinghua University Shenzhen, Guangdong, China

Tianqu Zhuang

zhuangtq23@mails.tsinghua.edu.cn
Tsinghua Shenzhen International Graduate School, Tsinghua University Shenzhen, Guangdong, China

Hao Wu

wu-h22@mails.tsinghua.edu.cn
Tsinghua Shenzhen International Graduate School, Tsinghua University Shenzhen ShenNong Information Technology Co., Ltd. Shenzhen, Guangdong, China

Yiheng Yang

2023311d15@stu.hit.edu.cn
Harbin Institute of Technology, Shenzhen, Shenzhen, Guangdong, China

Jiaxin Hong

acanghong425@gmail.com
Harbin Institute of Technology, Shenzhen, Shenzhen, Guangdong, China

Shu-Tao Xia

xiast@sz.tsinghua.edu.cn
Tsinghua Shenzhen International Graduate School, Tsinghua University Shenzhen, Guangdong, China

Abstract

Autoregressive image generation has witnessed rapid advancements, with prominent models such as scale-wise visual autoregression pushing the boundaries of visual synthesis. However, these developments also raise significant concerns regarding data privacy and copyright. In response, training data detection has emerged as a critical task for identifying unauthorized data usage in model training. To better understand the vulnerability of autoregressive image generative models to such detection, we conduct the first study that applies membership inference to this domain. Our approach comprises two key components: implicit classification and an adaptive score aggregation strategy. First, we compute the implicit token-wise classification score within the query image. Then we propose an adaptive score aggregation strategy to acquire a final score, which places greater emphasis on the tokens with lower scores. A higher final score indicates that the sample is more likely to be involved in the training set. Extensive experiments demonstrate the superiority of our method over those designed for

*Corresponding author.

Permission to make digital or hard copies of all or part of this work for personal or classroom use is granted without fee provided that copies are not made or distributed for profit or commercial advantage and that copies bear this notice and the full citation on the first page. Copyrights for components of this work owned by others than the author(s) must be honored. Abstracting with credit is permitted. To copy otherwise, or republish, to post on servers or to redistribute to lists, requires prior specific permission and/or a fee. Request permissions from permissions@acm.org.

MM '25, Dublin, Ireland

© 2025 Copyright held by the owner/author(s). Publication rights licensed to ACM. ACM ISBN 978-1-4503-XXXX-X/2018/06
<https://doi.org/XXXXXX.XXXXXXX>

LLMs, in both class-conditional and text-to-image scenarios. Moreover, our approach exhibits strong robustness and generalization under various data transformations. Furthermore, sufficient experiments suggest two novel key findings: (1) A linear scaling law on membership inference, exposing the vulnerability of large foundation models. (2) Training data from scale-wise visual autoregressive models is easier to detect than other autoregressive paradigms. Our code is available at <https://github.com/Chrisqewx/ImageAR-MIA>.

CCS Concepts

• Security and privacy → Privacy protections; • Computing methodologies → Computer vision.

Keywords

Training Data Detection, Membership Inference, Visual Autoregressive Model

ACM Reference Format:

Hongyao Yu, Yixiang Qiu, Yiheng Yang, Hao Fang, Tianqu Zhuang, Jiaxin Hong, Bin Chen, Hao Wu, and Shu-Tao Xia. 2025. ICAS: Detecting Training Data from Autoregressive Image Generative Models. In *Proceedings of the 33rd ACM International Conference on Multimedia (MM '25)*, October 27–31, 2025, Dublin, Ireland. ACM, New York, NY, USA, 14 pages. <https://doi.org/XXXXXX.XXXXXXX>

1 Introduction

In the past few years, autoregressive image generation has advanced rapidly, with scale-wise visual autoregression (VAR) [35] emerging as a prominent representative. VAR not only achieves superior image quality compared to diffusion models but also accelerates

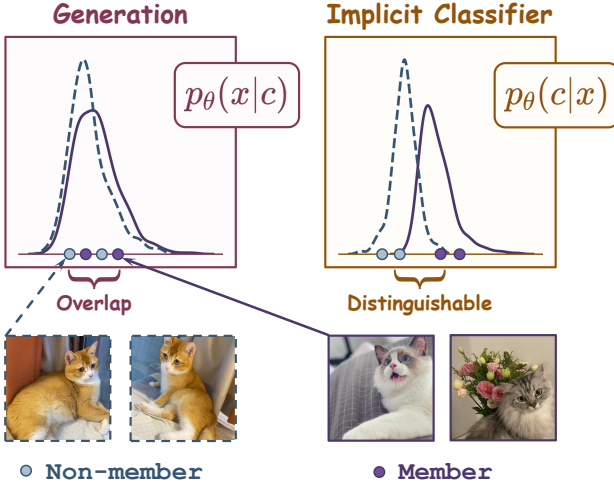


Figure 1: MI methods developed for LLMs, which leverage the generative probability, fail to distinguish the distribution shift between member and non-member samples. In contrast, the implicit classifier can distinguish them.

the image generation process, establishing it as a mainstream paradigm in image generation, alongside GANs and diffusion models [4, 35, 44]. However, the impressive generative capabilities of visual autoregressive models rely heavily on large-scale image datasets, primarily sourced from the web [19, 41]. This practice poses potential risks to privacy [10, 25, 26] and security [9, 40, 46]. Membership inference (MI) [6, 19, 32] has become a widely adopted technique for detecting unauthorized data usage during model training. This enables data owners to identify whether their data has been used in the training process without permission, which can lead to potential misuse or legal violations.

To fully understand the robustness of such models to protect their training data, we propose the first membership inference research specifically targeting VARs. Although this visual autoregressive paradigm shares similarities to autoregressive large language models (LLMs), the membership inference methods developed for LLMs [21, 32, 43] fail to perform effectively on autoregressive image models due to their strong generalization capabilities, as demonstrated in the left part of Figure 1.

To address this challenge, we introduce a novel membership inference method ICAS tailored for autoregressive image generative models. Unlike detection methods for LLMs that estimate the generation probability for a given condition, our approach considers the probability of the condition corresponding to the image, referred to as the implicit classification, which can effectively distinguish between member and non-member samples, as shown in Figure 1. Building upon this, we propose a membership inference method based on the implicit classifier (IC). Specifically, we first compute the implicit classification score of the image tokens in the query image. Next, we employ an adaptive score aggregation strategy (AS) to combine these token-level scores into a final score, which focuses more on low-score tokens. A higher final score indicates a greater likelihood that the image is included in the training data.

We conduct extensive experiments on various visual autoregressive models in different scenarios, including class-conditional and text-to-image generation. For comparison, we also implement detection methods designed for large language models, due to the similarities in the autoregressive paradigm. Our experimental results demonstrate that our proposed method outperforms existing detection methods for LLMs in detecting the training data of visual autoregressive models. Additionally, robustness analysis and ablation studies confirm the robustness and efficacy of our approach. We also explore the relationship between model size and detection performance, revealing a linear scaling law for membership inference in relation to model parameters, indicating that larger models are more vulnerable to membership inference. Moreover, we find that the detection from the scale-wise autoregressive model is much easier than other autoregressive paradigms.

We summarize our contributions as follows:

- We are the first to explore membership inference for training data detection in autoregressive image generative models. Our method contains an implicit classifier and an adaptive score aggregation strategy.
- Experimental results reveal that our methods outperform competitive baselines and demonstrate the robustness and generalizability of our method across various scenarios.
- We explore a linear scaling law for membership inference in autoregressive image generative models, and discover it is easier to detect training data on large or scale-wise visual autoregressive models.

2 Related Work

2.1 Membership Inference on Diffusion Models.

Recently, diffusion models have demonstrated superior performance in generative tasks [7, 30, 34]. To ensure that image data is not used without authorization, some membership inference [11, 22] algorithms have been proposed to detect whether images are used for model training. Naive Loss [22] attack is the first proposed to leverage the prediction loss on the random Gaussian loss to detect the training sample on diffusion models, which is implemented by comparing the distance between the Gaussian noise and the predicted noise. Proximal Initialization Attack (PIA) [18] advances the Naive Loss [22] by utilizing the predicted noise in the clean image instead of the random noise. In addition to using only the sample itself for evaluation, PFAMI [11] introduces the neighbor samples, acquired through image transformations. The research finds higher denoising loss gap between the origin sample and neighbor samples indicates higher likelihood for the member samples. Instead of detect from the original clean image, [6] proposes the SecMI method. They adopt the DDIM inversion technique to reverse the image to timestep t , and calculate the approximated posterior estimation error. Similarly, [19] also leverages the DDIM inversion result, they compute the SSIM metric between it and the clean image. [41] further identify the conditional overfitting phenomena, they compare the predicted noise with and without the corresponding condition for membership inference. However, although membership inference for image generation in diffusion models has been extensively studied, it cannot be directly transferred to autoregressive image generation, owing to its completely different generation paradigm.

2.2 Membership Inference on LLMs

In addition to image generative models, membership inference on large language models (LLMs) similarly attracts extensive attention from the research community. For instance, the Min- $k\%$ method [32] assumes that the member samples are less likely to contain outlier tokens with low log probabilities. They identify the $k\%$ tokens with the lowest log probabilities, averaging them to detect member samples. Building upon this foundational work, [43] further emphasizes the local maxima issue, considering that the ground-truth token is more likely to have a larger log probability than other tokens in a member sample. Instead of directly using the log probability, they subtract the average token probability score from the log probability of each token and normalize it. In contrast to methods based on the average probability of the lowest $k\%$ tokens, DC-PDD [45] leverages the divergence between the token probability distribution within the text and the token frequency distribution across the reference corpus to identify training data, which mitigates misclassification issues that arise when non-member texts contain numerous common tokens with high predicted probabilities. Instead of using the predicted probability, [27] proposes to calculate the infilling log likelihood for tokens. This method not only considers the preceding tokens but also incorporates subsequent ones for a more comprehensive and accurate analysis. Lastly, [42] explores the behavior gap in fine-tuning between member and non-member samples. Their findings show that the gap in log probability before and after fine-tuning is smaller for member samples compared to non-members.

2.3 Autoregressive Image Generative Models.

In recent years, the field of autoregressive image generation has developed rapidly, and a variety of autoregressive image generation paradigms have emerged. VQVAE [36] first demonstrates the ability to decompose a 2D image into 1D discrete token sequences. VQGAN [8] upgrade from VQVAE by introducing the perceptual and discriminator loss, as well as a raster-scan autoregressive transformer to generate image tokens. LlamaGen proposes to use the Llama transformer architecture to execute the raster-scan process, combining VQVAE and exceeding the stable diffusion model [30], and PAR [37] accelerates it by parallel decoding. MaskGIT [3] proposed a mask-based method, using a bidirectional transformer to predict the mask tokens. Beyond 1D raster scanning, NAR [13] predicts the neighbor tokens in all directions.

Among the many autoregressive generation paradigms, the scale-wise visual autoregressive model (VAR) [35] is an outstanding representative. [35] first proposes this generative paradigm. It leverages a multi-scale image tokenizer to transfer an image into image tokens with different scales. The transformer predicts the next-scale tokens with previous-scale tokens. There are many follow-up improvements based on this foundation work. VAR-CLIP [44] replace the class condition with CLIP embedding, extending it from class-condition generation to text-to-image generation. M-VAR [28] upgrade it with a mamba architecture [12]. CCA [4] considers the classifier-free guidance into training to avoid the extra cost for the guidance in the inference time. The rapid development and widespread adoption of this technology highlight the urgent need to study its privacy and security issues.

3 Method

3.1 Preliminaries

Membership Inference. Let \mathbb{D} be a dataset drawn from the real data distribution. The model owner uses a subset $\mathbb{D}_{mem} \subseteq \mathbb{D}$ to train a model. The remaining part is denoted as the hold-out dataset $\mathbb{D}_{out} = \mathbb{D} \setminus \mathbb{D}_{mem}$. In the context of conditional image generation models, each data point consists of an image \mathbf{x} and a corresponding condition c . The goal of a membership inference (MI) is to determine whether a given data point (\mathbf{x}, c) is used in the training of the image generator. The membership inference can mainly be divided into reference-based methods [2, 31, 38] and reference-free methods [21, 32, 43]. Reference-based methods typically require the training of shadow models on similar distributions. However, these approaches depend on prior knowledge of the training data, and the cost of training additional models makes them impractical for large-scale models [32]. Consequently, we focus on reference-free methods that do not require prior knowledge of the training data or the details of the training process. The membership inference algorithm for conditional image generation can be formulated as:

$$\mathcal{M}(\mathbf{x}, c) = \mathbf{1}[\text{Score}(\mathbf{x}, c) \geq \tau], \quad (1)$$

where $\mathcal{M}(\mathbf{x}, c) = 1$ means the data point (\mathbf{x}, c) is used to train the target model, τ is a threshold, and $\mathbf{1}[\cdot]$ is an indicator function.

Scale-wise Visual Autoregressive Models. Scale-wise Visual Autoregressive Model (VAR) [35] contains a multi-scale VQVAE and a visual autoregressive transformer.

The multi-scale VQVAE is used to tokenize the image into a series of discrete image token maps with K different scale levels. It includes an encoder \mathcal{E} , a decoder \mathcal{D} , and a quantizer Q with a codebook $Z \in \mathbb{R}^{V \times C}$, where V is the vocabulary size and C is the channel dimension. The encoder tokenizes the image \mathbf{x} into a feature map f_K :

$$f_K = \mathcal{E}(\mathbf{x}) \in \mathbb{R}^{C \times h_K \times w_K}, \quad (2)$$

where $h_K \times w_K$ is the latent resolution of the feature map. Then the feature map is quantized into K multi-scale token maps $R = (r_1, r_2, \dots, r_K)$. The r_k contains $h_k \times w_k$ tokens, and the number increases when the scale level k gets larger. The k -th residual map is defined as $f'_k = Z(r_k)$. The k -th feature map f_k is the cumulative sum of the residual maps:

$$f_k = \sum_{i=1}^k \text{Upsample}(f'_i, (h_k \times w_k)), \quad (3)$$

where $\text{Upsample}(f', (h \times w))$ means to resize the residual map f' into size $h \times w$ with bilinear upsampling function. The reconstructed image can be decoded with the last feature map:

$$\mathbf{x}' = \mathcal{D}(f_K). \quad (4)$$

The visual autoregressive transformer T_θ parameterized with weight θ is used to predict the next-scale token maps using tokens with lower scale levels:

$$p_\theta(r_k | c, r_1, \dots, r_{k-1}) = T_\theta(c, f_{k-1}^{\text{up}}) \quad (5)$$

$$f_{k-1}^{\text{up}} = \text{Upsample}(f_{k-1}, (h_k \times w_k)), \quad (6)$$

where c is the condition. The recursive formula of the feature map can also be written as:

$$f_k = Z(r_k) + \text{Upsample}(f_{k-1}, (h_k \times w_k)), \quad (7)$$

where r_k is sampled from $p_\theta(r_k|c, r_1, \dots, r_{k-1})$. In this paper, we focus on the membership inference on the visual autoregressive transformer.

3.2 Detection via Implicit Classifier

As outlined in Sec. 3.1, an image \mathbf{x} can be decomposed into K token maps (r_1, r_2, \dots, r_K) . Consequently, the likelihood of the image can be expressed as:

$$\begin{aligned} p_\theta(\mathbf{x}|c) &= \prod_{k=1}^K p_\theta(r_k|c, r_1, \dots, r_{k-1}) \\ &= \prod_{k=1}^K \prod_{i=1}^{h_k} \prod_{j=1}^{w_k} p_\theta(r_k^{(i,j)}|c, r_1, \dots, r_{k-1}), \end{aligned} \quad (8)$$

where $r_k^{(i,j)}$ represents the token with coordinates (i, j) on r_k . For simplicity, we expand all tokens into a sequence and ignore the conditions of the preceding token maps for simplicity so that the probability can be written as:

$$p_\theta(\mathbf{x}|c) = \prod_{i=1}^N p_\theta(x_i|c), \quad (9)$$

where $N = \sum_{k=1}^K h_k \times w_k$ is the total number of tokens.

To detect whether an image \mathbf{x} belongs to the training set, recent studies exploit an overfitting phenomenon. The overfitting issue manifests a higher prediction probability for the ground-truth tokens in the member set [32, 43]. However, this assumption fails when it comes to the visual autoregressive models, which exhibit strong generalization ability. As shown in the right portion of Figure 2, the distributions of log-likelihoods for tokens (*i.e.*, $p_\theta(x_i|c)$) from member samples and non-member samples are similar, making it challenging to differentiate between them.

Classifier-free guidance (CFG), as proposed by [16], involves comparing the model predictions with and without a specific condition, such as a class or a text condition. It utilizes an implicit classifier $p_\theta(c|\mathbf{x})$ to guide the generation, *i.e.*, $\tilde{p}_\theta(\mathbf{x}|c) = p_\theta(\mathbf{x}|c)p_\theta^\omega(c|\mathbf{x})$, where θ is the parameters of the generative model, and ω is the CFG ratio. The implicit classifier is implemented as follows:

$$p_\theta(c|\mathbf{x}) \propto \frac{p_\theta(\mathbf{x}|c)}{p_\theta(\mathbf{x})}. \quad (10)$$

The CFG guidance works by adjusting the generation process to push the result in the direction of high confidence for the target condition while avoiding regions that correspond to other classes. In the practice of the generation using diffusion models, the CFG ratio is typically set to a value like $7.5 \gg 1$, underscoring its significant role in conditional image generation. To validate this effect in visual autoregressive models, we use the VAR-d30 [35] trained on the training set of ImageNet [5] to generate 50000 images with a series of different CFG ratios. Then we calculate the FID score [15] of the generated images. We use two reference datasets to calculate FID, the training set (member) and the validation set (non-member), and the evaluation results are denoted as FID_{train} and FID_{val} . The

evaluation results presented in Figure 3 shows that a higher CFG ratio leads to a higher gap between FID_{train} and FID_{val} , which means that the distribution of the generated images is closer to the training set with the help of the classifier-free guidance. This finding further highlights a strong potential from the implicit classifier in distinguishing member samples from non-member samples.

Inspired by these findings, we propose an implicit classifier-based detection method. It leverages the difference between conditional and unconditional predicted probabilities to determine whether a sample is a member. Specifically, the method approximates the implicit classification score by:

$$\begin{aligned} \log p_\theta(c|\mathbf{x}) &\propto \log \frac{p_\theta(\mathbf{x}|c)}{p_\theta(\mathbf{x})} \\ &= \log \frac{\prod_{i=1}^N p_\theta(x_i|c)}{\prod_{i=1}^N p_\theta(x_i)} \\ &= \sum_{i=1}^N (\log p_\theta(x_i|c) - \log p_\theta(x_i)) \\ &\stackrel{\text{def.}}{=} \text{Score}(\mathbf{x}, c). \end{aligned} \quad (11)$$

Intuitively, the score is the accumulation of the difference between the conditional and unconditional log probability of each token, and the implicit classification score of each image token can be formulated as follows:

$$\text{Score}(x_i, c) = \log p_\theta(x_i|c) - \log p_\theta(x_i). \quad (12)$$

The right portion of Figure 2 demonstrates the effectiveness of the implicit classifier (*i.e.*, $p_\theta(c|x_i)$). The distribution of log probability with or without condition is similar between member samples and non-member samples, resulting in a low Area-Under-the-ROC-curve (AUROC). However, when we compute the implicit classification score, a clear distinction emerges between member and non-member samples, significantly improving the model's ability to distinguish between them. This demonstrates the power of our implicit classifier-based method in enhancing the detection performance of membership in visual autoregressive models.

3.3 Adaptive Score Aggregation Strategy

In the previous section, we defined the implicit classification score of each image token, and the overall score of the image as the sum of all token scores. However, the difficulty of predicting tokens for different images varies significantly. It is possible for a few tokens from non-member samples to receive high scores from the implicit classifier, with an example from Figure 4. These high-scoring tokens, though limited in number, can negatively impact the performance of membership inference. On the other hand, due to the overfitting phenomenon during training, the probability of low token scores in member samples tends to be smaller, while non-member samples generally have more tokens with low scores [32]. To address this issue and better distinguish between member and non-member samples, it is essential to assign more weight to tokens with lower scores and less weight to those with higher scores. To achieve this, we introduce a adaptive score aggregation approach, which puts

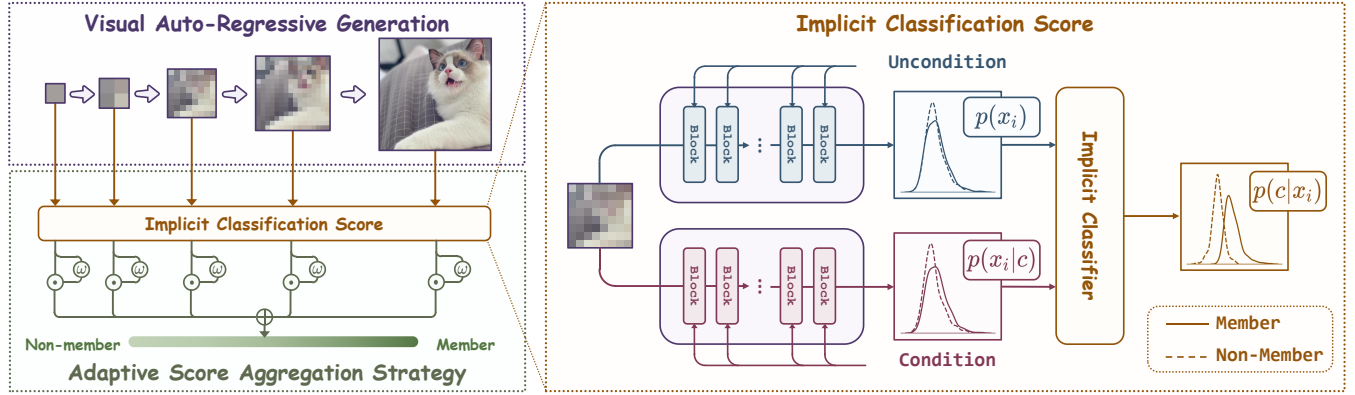


Figure 2: Overview of our membership inference method. The distribution is based on the experimental results of VAR-d24.

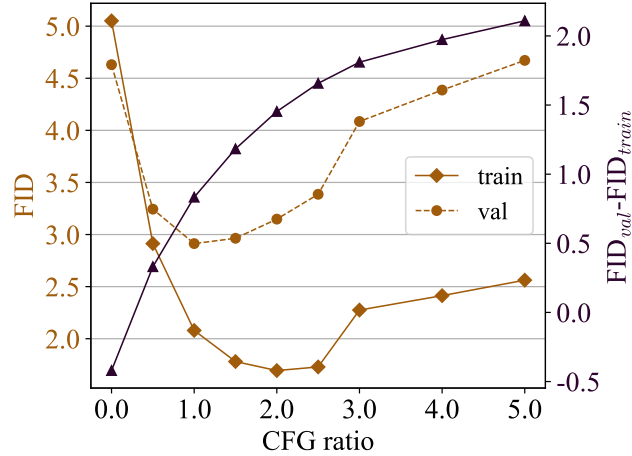


Figure 3: FID evaluation results with different CFG ratios on training set and validation set.

more emphasis on the tokens with lower scores:

$$\text{Score}(\mathbf{x}, c) = \sum_{i=1}^N \omega_i \cdot \text{Score}(x_i, c), \quad (13)$$

where $\omega_i > 0$ is the weight of the i -th token, and it should be larger when the $\text{Score}(x_i, c)$ comes lower. In practice, we define the weight ω_i as follows:

$$\omega_i = \frac{1}{a + \exp(b \cdot \text{Score}(x_i, c))}, \quad (14)$$

where $a > 0$ and $b > 0$ are hyperparameters. Therefore, the score of the total image can be formulated as:

$$\text{Score}(\mathbf{x}, c) = \sum_{i=1}^N \frac{1}{a + (\frac{\text{Score}(x_i|c)}{\text{Score}(x_i)})^b} \log \frac{p_\theta(x_i|c)}{p_\theta(x_i)}. \quad (15)$$

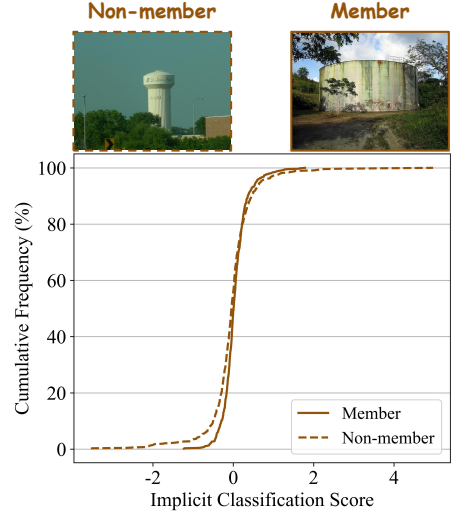


Figure 4: Cumulative distribution of token scores from a specific member and a non-member sample. A few tokens in the non-member sample have high scores, while more have low scores.

4 Experiments

4.1 Experimental Setup.

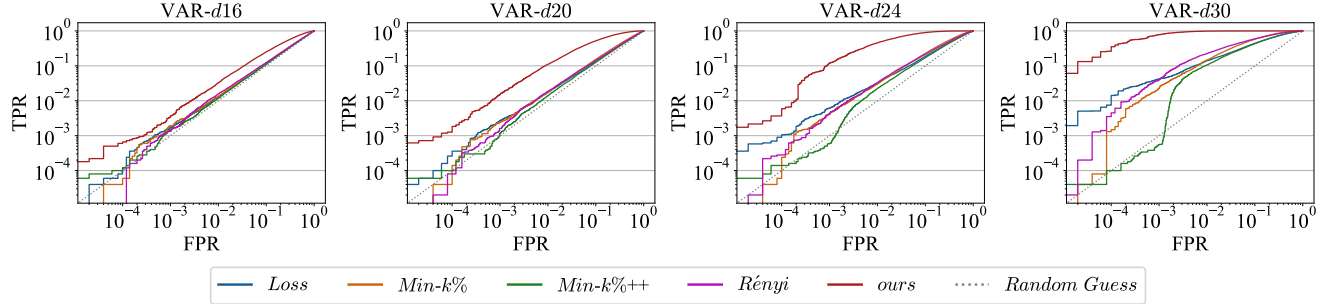
Target models and datasets. In the main paper, we utilize three prominent scale-wise visual autoregressive models, including VAR [35], VAR-CCA [4], and VAR-CLIP [44]. Inside them, VAR and VAR-CCA are class-conditional generative models, and VAR-CLIP is a text-to-image generative model. Moreover, VAR and VAR-CCA include four different model depths, *i.e.*, $\{d16, d20, d24, d30\}$, and a larger model depth means a larger model. We also conduct experiments on other types of autoregressive models for image generation, such as M-VAR [28], LlamaGen [33], LlamaGen-CCA [4], PAR [37], and NAR [13]. The results are provided in Appendix B. We conduct experiments on the models without further fine-tuning or other

Table 1: Experiment results in VAR models

Method	VAR-d16			VAR-d20			VAR-d24			VAR-d30		
	↑ AUROC	↑ TPR@5%	↑ ASR	↑ AUROC	↑ TPR@5%	↑ ASR	↑ AUROC	↑ TPR@5%	↑ ASR	↑ AUROC	↑ TPR@5%	↑ ASR
<i>Loss</i>	0.5223	0.0580	0.5163	0.5468	0.0707	0.5332	0.6027	0.1058	0.5752	0.7754	0.3084	0.7090
<i>Min-k%</i>	0.5366	0.0653	0.5244	0.5813	0.0798	0.5570	0.6648	0.1261	0.6186	0.8593	0.4095	0.7803
<i>Min-k%++</i>	0.5213	0.0572	0.5140	0.5402	0.0659	0.5267	0.5941	0.0938	0.5676	0.7778	0.2919	0.7039
<i>Rényi</i>	0.5315	0.0660	0.5211	0.5577	0.0784	0.5412	0.6332	0.1251	0.5948	0.8520	0.4597	0.7681
<i>ICAS(ours)</i>	0.6838	0.1417	0.6345	0.8402	0.3494	0.7628	0.9624	0.7824	0.9001	0.9990	0.9997	0.9897

Table 2: Experiment results in VAR-CCA models

Method	VAR-CCA-d16			VAR-CCA-d20			VAR-CCA-d24			VAR-CCA-d30		
	↑ AUROC	↑ TPR@5%	↑ ASR	↑ AUROC	↑ TPR@5%	↑ ASR	↑ AUROC	↑ TPR@5%	↑ ASR	↑ AUROC	↑ TPR@5%	↑ ASR
<i>Loss</i>	0.5310	0.0689	0.5217	0.5702	0.1025	0.5493	0.6737	0.2306	0.6266	0.9177	0.7483	0.8516
<i>Min-k%</i>	0.5543	0.0697	0.5382	0.6321	0.0934	0.5947	0.7908	0.1918	0.7257	0.9774	0.8751	0.9427
<i>Min-k%++</i>	0.5135	0.0504	0.510	0.5148	0.0485	0.5137	0.5074	0.0646	0.5109	0.6039	0.1333	0.5871
<i>Rényi</i>	0.5180	0.0609	0.5120	0.5407	0.0782	0.5272	0.6022	0.1382	0.5717	0.8326	0.5369	0.7607
<i>ICAS(ours)</i>	0.6032	0.1016	0.5780	0.7642	0.2463	0.7049	0.9279	0.6605	0.8583	0.9980	0.9969	0.9869

**Figure 5: The log ROC curve for membership inference on the VAR models**

modifications. All the models are trained on the training set of ImageNet [5] with 1000 classes.

Evaluation Metrics. Following previous researches [19, 32], to evaluate our method, we adopt the widely used metrics, including Area-Under-the-ROC-curve (AUROC), and the True Positive Rate when the False Positive Rate is 5% (TPR@5%), and attack success rate (ASR). For ASR, we randomly select a subset of both member and non-member samples, comprising 20% of the total, and compute an optimal threshold from it. Then we apply the threshold to evaluate the ASR for the remaining samples.

Baselines. Since the autoregressive generation paradigm in visual autoregressive models is similar to the text generation paradigm, we adapt some advanced training data detection methods for large language models as our baseline. Specifically, we adapt the *Loss* attack [39], *Min-k%* [32], *Min-k%++* [43] and *Rényi* entropy score [21] in our experiments. The implementation detail for baselines is provided in Appendix A.

Implementation Details. We use the first 50 images for each class in the training set as the member dataset \mathbb{D}_{mem} , and the validation set of ImageNet is supported as the hold-out dataset \mathbb{D}_{out} . In total, we have 50000 member samples and 50000 non-member samples. For baselines, we carefully adjust their hyperparameters

and select the best ones in each setting. For our method, we set $a = 1.75$ and $b = 1.3$ in the adaptive score aggregation strategy.

4.2 Comparison to Baselines

Evaluation on Class-Condition Generation. Table 1 and 2 shows the experimental results on the VAR and VAR-CCA models with different model depths, respectively. Compared to the baseline methods, our method consistently outperforms all other approaches across all evaluation metrics and model variants. Particularly, when the model depth is small (e.g., 16 and 20), the baseline algorithms exhibit minimal effectiveness, performing only slightly better than random guessing. In contrast, our method demonstrates strong distinguishability between member and non-member samples. Notably, it achieves 0.1472 and 0.2589 increase on AUROC for VAR models with depths 16 and 20, respectively. As the model depth increases, such as in the case of VAR-d30, the AUROC scores exceed 0.9980, indicating that the effective detection performance for larger models. These results clearly show that our method is highly effective in distinguishing training data from non-training data across all variants of the VAR model.

The log ROC curve for detection on the VAR models is shown in Figure 5. It is evident that baseline methods sometimes yield

lower TPR than random guessing, especially when the FPR is low. In these cases, the True Positive Rate (TPR) of the baseline methods can be almost indistinguishable from a random guess, indicating their limited ability to correctly classify training data. In contrast, our method demonstrates significantly superior performance, consistently achieving a much higher True Positive Rate (TPR), even at low False Positive Rates (FPRs). The ROC curve for our approach clearly shows a marked separation from the baseline methods, illustrating the effectiveness of our method in distinguishing between member and non-member samples. This strong distinguishability is particularly evident across different model depths, highlighting the effectiveness and reliability of our approach.

Evaluation on Text-to-Image Generation. Table 3 presents the membership inference results on the VAR-CLIP model. In this scenario, our detection method achieves an AUROC of 0.8817, significantly outperforming the baseline methods. Moreover, when compared to the class-conditional generation scenario (*i.e.*, VAR), the AUROC of our method shows an impressive improvement of 0.2. This substantial gap highlights a key observation: the text generation model exhibits a strong overfitting characteristic to the training text, which makes the model particularly vulnerable to membership inference. This vulnerability is a direct consequence of the model’s reliance on the specific training data, further reinforcing the effectiveness of our method in detecting training data in the context of text-to-image generative models.

Table 3: Experiment results in VAR-CLIP

Method	VAR-CLIP		
	↑ AUROC	↑ TPR@5%	↑ ASR
<i>Loss</i>	0.5537	0.0776	0.5370
<i>Min-k%</i>	0.6109	0.0894	0.5784
<i>Min-k%++</i>	0.5356	0.0624	0.5246
<i>Rényi</i>	0.5549	0.0716	0.5384
<i>ICAS(ours)</i>	0.8817	0.3989	0.8024

4.3 Robustness Evaluation

In real-world scenarios, images are often subjected to various disturbances such as rotation, noise, and other transformations. These factors introduce a certain offset between the original images and the member images used for detection. As a result, it becomes essential to evaluate the robustness of the membership inference under image perturbations to understand its effectiveness in practical settings. Similar to previous work [19], we apply four common image transformations to disrupt the original images and test the robustness of our membership inferences:

- **Additional Noise.** Gaussian noise with a standard deviation of 0.1 is added to the original images, introducing random noise and making the image less clear. Note that the noise is fixed when applying to different images.
- **Rotation.** Images are rotated by 10 degrees around the geometric midpoint.

- **Saturation.** The saturation levels of images are increased to 150% or decreased to 50%, affecting the color intensity and making the image either more vivid or dull.

- **Brightness.** The brightness of images are increased or decreased by 50%, affecting the overall lightness or darkness of the images.

These perturbations simulate real-world scenarios in which images may undergo various transformations, helping to assess how robust our method are in the presence of such challenges. The results are shown in Figure 6. We observe that the AUROC values of different detection algorithms experience varying degrees of decline due to these transformations. Since such perturbations are not part of the training process for the VAR model, transformed member images are not used during training, increasing the difficulty for the detection methods.

However, our proposed method demonstrates exceptional resilience against various types of image transformations, while baseline methods exhibit poor robustness. The experimental results highlight the superior stability and robustness of our approach when confronted with diverse distortions encountered in real-world settings. Specifically, our method maintains a high level of accuracy despite the presence of noise, rotation, and changes in brightness or saturation. This underscores not only the robustness of our method but also its potential applicability in dynamic environments where image transformations are commonplace. Such resilience ensures that our approach remains effective even in challenging, noisy, or altered conditions, setting it apart from baseline methods that struggle to adapt to these real-world distortions.

4.4 Ablation Study

This part provides ablation studies to analyze the role of each component in our detection method. We conduct the experiments using VAR with different model depths.

Table 4: Ablation study of the implicit classifier (IC) in VAR

Model	↑ AUROC		↑ TPR@5%		↑ ASR	
	w IC	w/o IC	w IC	w/o IC	w IC	w/o IC
VAR-d16	0.6838	0.5463	0.1417	0.0618	0.6345	0.5340
VAR-d20	0.8402	0.6031	0.3494	0.0889	0.7628	0.5748
VAR-d24	0.9624	0.6868	0.7824	0.1368	0.9001	0.6355
VAR-d30	0.9990	0.8266	0.9997	0.3076	0.9897	0.7505

Implicit Classifier. The implicit classifier plays a crucial role in our detection. In Table 4, we present the results of an ablation study that evaluates the impact of removing the implicit classifier. The results show a significant drop in detection performance when the implicit classifier is removed, emphasizing its importance in the overall effectiveness of our approach. This finding reinforces the fact that the implicit classifier plays a vital role in enhancing the discriminative power in the training data detection.

Adaptive Score Aggregation Strategy. We conduct an ablation study on the weighted aggregation strategy. By observing the results presented in Table 5, we find that removing the weight adjustment strategy leads to a substantial decline in detection performance. This underscores the importance of the weight aggregation

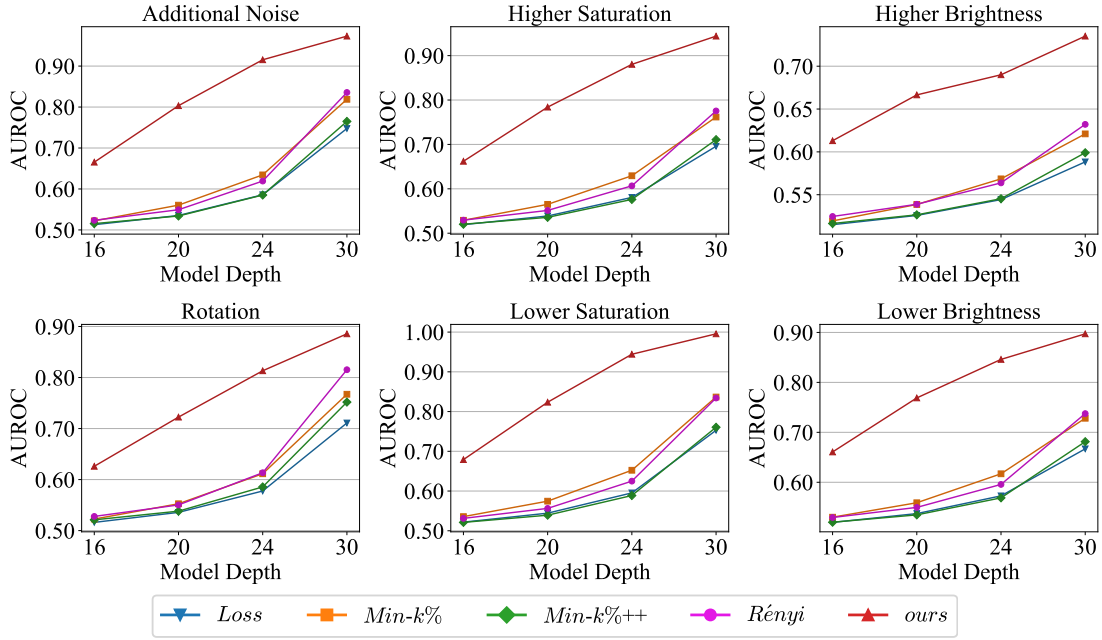


Figure 6: Experimental results on different image transformations

Table 5: Ablation study of the Adaptive Score Aggregation Strategy (AS) in VAR

Model	↑ AUROC		↑ TPR@5%		↑ ASR	
	w AS	w/o AS	w AS	w/o AS	w AS	w/o AS
VAR-d16	0.6838	0.6354	0.1417	0.0856	0.6345	0.6001
VAR-d20	0.8402	0.7793	0.3494	0.1826	0.7628	0.7133
VAR-d24	0.9624	0.9303	0.7824	0.5643	0.9001	0.8613
VAR-d30	0.9990	0.9955	0.9997	0.9969	0.9897	0.9787

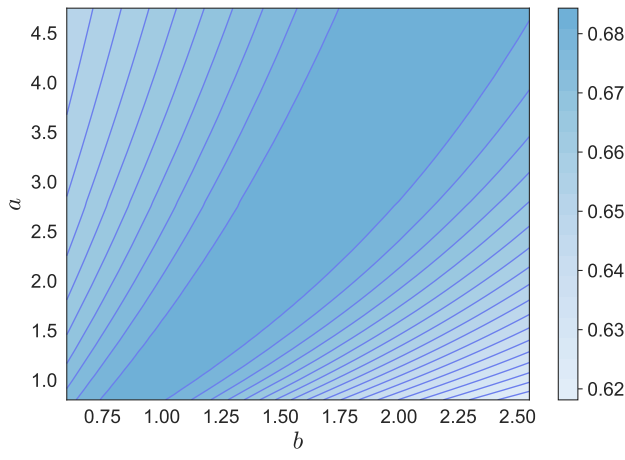


Figure 7: AUROC score with different hyperparameters

approach in our method, highlighting its contribution to improving the performance of the membership inference.

To gain further insight into the impact of this strategy's hyperparameters, we examine the AUROC scores under different parameter settings, as shown in Figure 7. The results indicate that the AUROC score remains relatively stable within a certain range of hyperparameters. Optional hyperparameters are $a = 1.75$ and $b = 1.3$, and we use them in our main experiments.

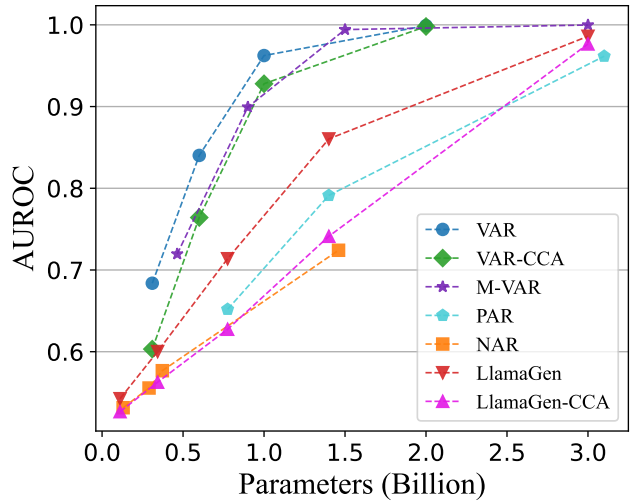


Figure 8: AUROC score with different model size

4.5 MI Linear Scaling Law

Previous research has established that scaling up autoregressive models such as LLMs [1, 14, 17] and VAR [35] follows a power-law scaling law like $L = (\beta X)^\alpha$, where X is controllable factors such as model parameters or training tokens, L is the evaluation result like test loss [1] or token error rate [35].

To explore whether similar scaling laws exist for membership inference, we extend our experiments to various paradigms of autoregressive image generative models with different model sizes, ranging from $111M$ to $3.1B$ parameters. The models under consideration include VAR [35], VAR-CCA [4], M-VAR [28], PAR [37], NAR [13], LlamaGen [33], and LlamaGen-CCA [4]. We apply our membership inference method to these autoregressive models of varying sizes, and the AUROC scores are presented in Figure 8. We can observe that when AUROC is not close to 1, e.g., below 0.98, it has a linear scaling law with the model parameters:

$$\text{AUROC} = \alpha P + \beta, \quad (16)$$

where P is the number of model parameters in billions. For example:

$$\begin{aligned} \text{AUROC}_{\text{NAR}} &= 0.143P + 0.517 \quad r = 0.998 \\ \text{AUROC}_{\text{LlamaGen-CCA}} &= 0.157P + 0.511 \quad r = 0.999, \end{aligned} \quad (17)$$

where r represents the correlation coefficient. This linear scaling law highlights the vulnerability of large autoregressive generative models to membership inference.

Compared to other autoregressive image generative paradigms, we discover that it is easier to detect the training data on the scale-wise visual autoregressive models (*i.e.*, VAR, VAR-CCA, and M-VAR), given the higher AUROC score. This significant phenomenon can be attributed to how these models process and generate visual data across multiple scales. The granular generation process in scale-wise models may increase the likelihood of memorizing specific details from the training set, thereby making them more susceptible to membership inference.

5 Conclusion

In this paper, we explore the training data detection on autoregressive image generative models for the first time. To detect whether an image is used to train the generative model, we first leverage an implicit classifier to calculate scores for all image tokens. Then we propose an adaptive score aggregation strategy to aggregate all token scores into a final score. The member samples tend to achieve higher final scores. Experimental results show that our method outperformed baselines designed in the text autoregressive generative domains. Robustness and ablation studies demonstrate the robustness and effectiveness of our method. Moreover, we discover a linear scaling law on membership inference and find the significant vulnerability of scale-wise visual autoregressive models.

References

- [1] Josh Achiam, Steven Adler, Sandhini Agarwal, Lama Ahmad, Ilge Akkaya, Florencia Leoni Aleman, Diogo Almeida, Janko Altenschmidt, Sam Altman, Shyamal Anadkat, et al. 2023. Gpt-4 technical report. *arXiv preprint arXiv:2303.08774* (2023).
- [2] Nicholas Carlini, Steve Chien, Milad Nasr, Shuang Song, Andreas Terzis, and Florian Tramer. 2022. Membership inference attacks from first principles. In *2022 IEEE symposium on security and privacy (SP)*. IEEE, 1897–1914.
- [3] Huiwen Chang, Han Zhang, Lu Jiang, Ce Liu, and William T Freeman. 2022. Maskgit: Masked generative image transformer. In *Proceedings of the IEEE/CVF conference on computer vision and pattern recognition*. 11315–11325.
- [4] Huayu Chen, Hang Su, Peize Sun, and Jun Zhu. 2024. Toward Guidance-Free AR Visual Generation via Condition Contrastive Alignment. *arXiv preprint arXiv:2410.09347* (2024).
- [5] Jia Deng, Wei Dong, Richard Socher, Li-Jia Li, Kai Li, and Li Fei-Fei. 2009. Imagenet: A large-scale hierarchical image database. In *2009 IEEE conference on computer vision and pattern recognition*. Ieee, 248–255.
- [6] Jinhao Duan, Fei Kong, Shiqi Wang, Xiaoshuang Shi, and Kaidi Xu. 2023. Are diffusion models vulnerable to membership inference attacks? In *International Conference on Machine Learning*. PMLR, 8717–8730.
- [7] Patrick Esser, Sumith Kulal, Andreas Blattmann, Rahim Entezari, Jonas Müller, Harry Saini, Yam Levi, Dominik Lorenz, Axel Sauer, Frederic Boesel, et al. 2024. Scaling rectified flow transformers for high-resolution image synthesis. In *Forty-first international conference on machine learning*.
- [8] Patrick Esser, Robin Rombach, and Björn Ommer. 2021. Taming transformers for high-resolution image synthesis. In *Proceedings of the IEEE/CVF conference on computer vision and pattern recognition*. 12873–12883.
- [9] Hao Fang, Bin Chen, Xuan Wang, Zhi Wang, and Shu-Tao Xia. 2023. Gifd: A generative gradient inversion method with feature domain optimization. In *Proceedings of the IEEE/CVF International Conference on Computer Vision*. 4967–4976.
- [10] Hao Fang, Yixiang Qiu, Hongyao Yu, Wenbo Yu, Jiawei Kong, Baoli Chong, Bin Chen, Xuan Wang, Shu-Tao Xia, and Ke Xu. 2024. Privacy leakage on dnns: A survey of model inversion attacks and defenses. *arXiv preprint arXiv:2402.04013* (2024).
- [11] Wenjie Fu, Huadong Wang, Chen Gao, Guanghua Liu, Yong Li, and Tao Jiang. 2023. A probabilistic fluctuation based membership inference attack for diffusion models. *arXiv preprint arXiv:2308.12143* (2023).
- [12] Albert Gu and Tri Dao. 2023. Mamba: Linear-time sequence modeling with selective state spaces. *arXiv preprint arXiv:2312.00752* (2023).
- [13] Yefei He, Yuanyu He, Shaoxuan He, Feng Chen, Hong Zhou, Kaipeng Zhang, and Bohan Zhuang. 2025. Neighboring Autoregressive Modeling for Efficient Visual Generation. *arXiv preprint arXiv:2503.10696* (2025).
- [14] Tom Henighan, Jared Kaplan, Mor Katz, Mark Chen, Christopher Hesse, Jacob Jackson, Heewoo Jun, Tom B Brown, Prafulla Dhariwal, Scott Gray, et al. 2020. Scaling laws for autoregressive generative modeling. *arXiv preprint arXiv:2010.14701* (2020).
- [15] Martin Heusel, Hubert Ramsauer, Thomas Unterthiner, Bernhard Nessler, and Sepp Hochreiter. 2017. Gans trained by a two time-scale update rule converge to a local nash equilibrium. *Advances in neural information processing systems* 30 (2017).
- [16] Jonathan Ho and Tim Salimans. 2022. Classifier-free diffusion guidance. *arXiv preprint arXiv:2207.12598* (2022).
- [17] Jared Kaplan, Sam McCandlish, Tom Henighan, Tom B Brown, Benjamin Chess, Rewon Child, Scott Gray, Alec Radford, Jeffrey Wu, and Dario Amodei. 2020. Scaling laws for neural language models. *arXiv preprint arXiv:2001.08361* (2020).
- [18] Fei Kong, Jinhao Duan, RuiPeng Ma, Hengtao Shen, Xiaofeng Zhu, Xiaoshuang Shi, and Kaidi Xu. 2023. An efficient membership inference attack for the diffusion model by proximal initialization. *arXiv preprint arXiv:2305.18355* (2023).
- [19] Qiao Li, Xiaomeng Fu, Xi Wang, Jin Liu, Xingyu Gao, Jiao Dai, and Jizhong Han. 2024. Unveiling structural memorization: Structural membership inference attack for text-to-image diffusion models. In *Proceedings of the 32nd ACM International Conference on Multimedia*. 10554–10562.
- [20] Xiang Li, Kai Qiu, Hao Chen, Jason Kuen, Zhe Lin, Rita Singh, and Bhiksha Raj. 2024. Controlvar: Exploring controllable visual autoregressive modeling. *arXiv preprint arXiv:2406.09750* (2024).
- [21] Zhan Li, Yongtao Wu, Yihang Chen, Francesco Tonin, Elias Abad Rocamora, and Volkan Cevher. 2024. Membership Inference Attacks against Large Vision-Language Models. *Advances in Neural Information Processing Systems* 37 (2024), 98645–98674.
- [22] Tomoya Matsumoto, Takayuki Miura, and Naoto Yanai. 2023. Membership inference attacks against diffusion models. In *2023 IEEE Security and Privacy Workshops (SPW)*. IEEE, 77–83.
- [23] Jiteng Mu, Nuno Vasconcelos, and Xiaolong Wang. 2025. EDITAR: Unified Conditional Generation with Autoregressive Models. *arXiv preprint arXiv:2501.04699* (2025).
- [24] Kai Qiu, Xiang Li, Hao Chen, Jie Sun, Jinglu Wang, Zhe Lin, Marios Savvides, and Bhiksha Raj. 2024. Efficient autoregressive audio modeling via next-scale prediction. *arXiv preprint arXiv:2408.09027* (2024).
- [25] Yixiang Qiu, Hao Fang, Hongyao Yu, Bin Chen, MeiKang Qiu, and Shu-Tao Xia. 2024. A closer look at gan priors: Exploiting intermediate features for enhanced model inversion attacks. In *European Conference on Computer Vision*. Springer, 109–126.
- [26] Yixiang Qiu, Hongyao Yu, Hao Fang, Wenbo Yu, Bin Chen, Xuan Wang, Shu-Tao Xia, and Ke Xu. 2024. Mibench: A comprehensive benchmark for model inversion attack and defense. *arXiv preprint arXiv:2410.05159* (2024).

[27] Negin Raoof, Litu Rout, Giannis Daras, Sujay Sanghavi, Constantine Caramanis, Sanjay Shakkottai, and Alex Dimakis. [n. d.]. Infilling Score: A Pretraining Data Detection Algorithm for Large Language Models. In *The Thirteenth International Conference on Learning Representations*.

[28] Sucheng Ren, Yaodong Yu, Nataniel Ruiz, Feng Wang, Alan Yuille, and Cihang Xie. 2024. M-VAR: Decoupled Scale-wise Autoregressive Modeling for High-Quality Image Generation. *arXiv preprint arXiv:2411.10433* (2024).

[29] Alfréd Rényi. 1961. On measures of entropy and information. In *Proceedings of the fourth Berkeley symposium on mathematical statistics and probability, volume 1: contributions to the theory of statistics*, Vol. 4. University of California Press, 547–562.

[30] Robin Rombach, Andreas Blattmann, Dominik Lorenz, Patrick Esser, and Björn Ommer. 2022. High-resolution image synthesis with latent diffusion models. In *Proceedings of the IEEE/CVF conference on computer vision and pattern recognition*. 10684–10695.

[31] Haonan Shi, Tu Ouyang, and An Wang. 2024. Learning-based difficulty calibration for enhanced membership inference attacks. In *2024 IEEE 9th European Symposium on Security and Privacy (EuroS&P)*. IEEE, 62–77.

[32] Weiji Shi, Anirudh Ajith, Mengzhou Xia, Yangsibo Huang, Daogao Liu, Terra Blevins, Danqi Chen, and Luke Zettlemoyer. 2023. Detecting pretraining data from large language models. *arXiv preprint arXiv:2310.16789* (2023).

[33] Peize Sun, Yi Jiang, Shoufa Chen, Shilong Zhang, Bingyue Peng, Ping Luo, and Zehuan Yuan. 2024. Autoregressive model beats diffusion: Llama for scalable image generation. *arXiv preprint arXiv:2406.06525* (2024).

[34] K Team. 2024. Kolors: Effective training of diffusion model for photorealistic text-to-image synthesis. *arXiv preprint* (2024).

[35] Keyu Tian, Yi Jiang, Zehuan Yuan, Bingyue Peng, and Liwei Wang. 2024. Visual autoregressive modeling: Scalable image generation via next-scale prediction. *Advances in neural information processing systems* 37 (2024), 84839–84865.

[36] Aaron Van Den Oord, Oriol Vinyals, et al. 2017. Neural discrete representation learning. *Advances in neural information processing systems* 30 (2017).

[37] Yuqing Wang, Shuhuai Ren, Zhijie Lin, Yujin Han, Haoyuan Guo, Zhenheng Yang, Difan Zou, Jiashi Feng, and Xihui Liu. 2024. Parallelized Autoregressive Visual Generation. *arXiv preprint arXiv:2412.15119* (2024).

[38] Lauren Watson, Chuan Guo, Graham Cormode, and Alex Sablayrolles. 2021. On the importance of difficulty calibration in membership inference attacks. *arXiv preprint arXiv:2111.08440* (2021).

[39] Samuel Yeom, Irene Giacomelli, Matt Fredrikson, and Somesh Jha. 2018. Privacy risk in machine learning: Analyzing the connection to overfitting. In *2018 IEEE 31st computer security foundations symposium (CSF)*. IEEE, 268–282.

[40] Hongyao Yu, Yixiang Qiu, Hao Fang, Bin Chen, Sijin Yu, Bin Wang, Shu-Tao Xia, and Ke Xu. 2024. Calor: Towards comprehensive model inversion defense. *arXiv preprint arXiv:2410.05814* (2024).

[41] Shengfang Zhai, Huanran Chen, Yinpeng Dong, Jiajun Li, Qingni Shen, Yansong Gao, Hang Su, and Yang Liu. 2024. Membership inference on text-to-image diffusion models via conditional likelihood discrepancy. *Advances in Neural Information Processing Systems* 37 (2024), 74122–74146.

[42] Hengxiang Zhang, Songxin Zhang, Bingyi Jing, and Hongxin Wei. 2024. Fine-tuning can Help Detect Pretraining Data from Large Language Models. *arXiv preprint arXiv:2410.10880* (2024).

[43] Jingyang Zhang, Jingwei Sun, Eric Yeats, Yang Ouyang, Martin Kuo, Jianyi Zhang, Hao Frank Yang, and Hai Li. 2024. Min-k%++: Improved baseline for detecting pre-training data from large language models. *arXiv preprint arXiv:2404.02936* (2024).

[44] Qian Zhang, Xiangzi Dai, Ninghua Yang, Xiang An, Ziyong Feng, and Xingyu Ren. 2024. Var-clip: Text-to-image generator with visual auto-regressive modeling. *arXiv preprint arXiv:2408.01181* (2024).

[45] Weichao Zhang, Ruqing Zhang, Jiafeng Guo, Maarten de Rijke, Yixing Fan, and Xueqi Cheng. 2024. Pretraining data detection for large language models: A divergence-based calibration method. *arXiv preprint arXiv:2409.14781* (2024).

[46] Tianqu Zhuang, Hongyao Yu, Yixiang Qiu, Hao Fang, Bin Chen, and Shu-Tao Xia. [n. d.]. Stealthy Shield Defense: A Conditional Mutual Information-Based Approach against Black-Box Model Inversion Attacks. In *The Thirteenth International Conference on Learning Representations*.

A Implement of Baselines

Since the autoregressive paradigm between visual autoregressive models and large language models is similar, we adopt some membership inference attacks designed for large language models as our baselines.

A.1 Loss Attack

The *Loss* attack method proposed by [39] predicts the membership of a sample using the training loss of the target model. In the training process, the cross-entropy (CE) loss will be used to train the model. To adapt it into autoregressive image generative models, we set the score of a single image token x_i as:

$$\text{Score}(x_i, c) = \log p_\theta(x_i|c), \quad (18)$$

where c is the condition, and p_θ is the prediction probability from the target model. The final score is the sum of token scores:

$$\text{Score}(\mathbf{x}, c) = \sum_{i=1}^N \text{Score}(x_i, c), \quad (19)$$

where N is the number of image tokens.

A.2 Min-k%

The token score of the *Min-k%* method [32] is the same as the *Loss* attack. Then, it selects the $k\%$ tokens with the lowest score, denoted as \mathbf{S}_{min} , where k is a hyperparameter. The final score is defined as the sum of the scores from the selected tokens:

$$\text{Score}(\mathbf{x}, c) = \sum_{i \in \mathbf{S}_{min}} \text{Score}(x_i, c). \quad (20)$$

A.3 Min-k%++

The *Min-k%* method [43] is an upgrade from *Min-k%*. It considers the expected probability of all tokens within the vocabulary. The token score is:

$$\text{Score}(x_i, c) = \frac{\log p_\theta(x_i|c) - \mu_{\cdot|c}}{\sigma_{\cdot|c}}, \quad (21)$$

where the $\mu_{\cdot|c}$ and $\sigma_{\cdot|c}$ are the expectation and the standard deviation of the tokens' log probability over the vocabulary. The formulation is as follows:

$$\begin{aligned} \mu_{\cdot|c} &= \mathbb{E}_{x \sim p_\theta(\cdot|c)} [\log p_\theta(x|c)] \\ \sigma_{\cdot|c} &= \sqrt{\mathbb{E}_{x \sim p_\theta(\cdot|c)} [(\log p_\theta(x|c) - \mu_{\cdot|c})^2]} \end{aligned} \quad (22)$$

The aggregation of the token scores is the same as the *Min-k%* method.

A.4 Rényi

This method [21] calculates the token scores leveraging the *Rényi* entropy [29] of order α (a hyperparameter):

$$\text{Score}(x_i, c) = \frac{1}{1-\alpha} \log \sum_{x \in V} (p_\theta^\alpha(x|c)), \quad (23)$$

where V is the vocabulary. When $\alpha = 1$, the token score is defined as:

$$\text{Score}(x_i, c) = - \sum_{x \in V} p(x|c) \log p(x|c). \quad (24)$$

And when $\alpha = +\infty$, they can be calculated as:

$$\text{Score}(x_i, c) = - \log \max_{x \in V} p(x|c). \quad (25)$$

Then, the method selects the $k\%$ tokens with the highest token scores, denoted as \mathbf{S}_{max} , where k is a hyperparameter. The final score is defined as the sum of the scores from the selected tokens:

$$\text{Score}(\mathbf{x}, c) = \sum_{i \in \mathbf{S}_{max}} \text{Score}(x_i, c). \quad (26)$$

B More Experimental Results

Instead of the scale-wise visual autoregressive models like VAR and VAR-CCA, we also extend our detection methods to other autoregressive image generative models, including M-VAR (Table 6 and 7), PAR (Table 8), NAR (Table 9 and 10), LlamaGen (Table 11 and 12) and LlamaGen-CCA (Table 13 and 14). All the results indicate our best performance on detecting training data of autoregressive generative models.

C MI Scaling Law on Other Perspectives

C.1 The number of scales and token counts

We explore the linear relationship between the AUROC and the use number of scales k or the log of the token count L . The results are presented in the left of Fig. 9, and they can be approximately fitted as:

$$\text{AUROC} = 0.0184k + 0.5122 \quad r = 0.9864$$

$$\text{AUROC} = 0.0189 \log_2 L + 0.5057 \quad r = 0.9980.$$

C.2 Baseline methods

To explore whether the baseline methods also satisfies the scaling law, we conduct experiments on VAR with different baselines. The results are shown in the right of Fig. 9, and they can be approximately fitted as:

$$\text{AUROC}_{\text{Loss}} = 0.1538P + 0.4614 \quad r = 0.9946$$

$$\text{AUROC}_{\text{Min-k\%}} = 0.1934P + 0.4715 \quad r = 0.9995$$

$$\text{AUROC}_{\text{Min-k\%++}} = 0.1571P + 0.4547 \quad r = 0.9904$$

$$\text{AUROC}_{\text{R\'enyi}} = 0.1959P + 0.4521 \quad r = 0.9939.$$

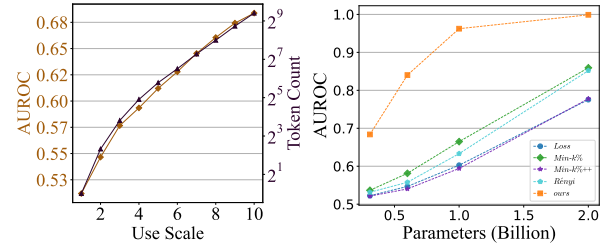


Figure 9: (Left) The AUROC and token count of VAR-d16 when using different number of scales. **(Right)** The scaling law of AUROC with different methods.

Table 6: Experiment results in M-VAR models (Part 1).

Method	M-VAR-d16			M-VAR-d20		
	\uparrow AUROC	\uparrow TPR@5%	\uparrow ASR	\uparrow AUROC	\uparrow TPR@5%	\uparrow ASR
<i>Loss</i>	0.5274	0.0594	0.5201	0.5644	0.0797	0.5462
<i>Min-k%</i>	0.5471	0.0683	0.5319	0.6109	0.0963	0.5795
<i>Min-k%++</i>	0.5232	0.0581	0.5147	0.5547	0.0714	0.5355
<i>Rényi</i>	0.5333	0.0669	0.5241	0.5792	0.0916	0.5555
<i>ICAS(ours)</i>	0.7196	0.1792	0.6627	0.8993	0.5132	0.8202

Table 7: Experiment results in M-VAR models (Part 2).

Method	M-VAR-d24			M-VAR-d32		
	\uparrow AUROC	\uparrow TPR@5%	\uparrow ASR	\uparrow AUROC	\uparrow TPR@5%	\uparrow ASR
<i>Loss</i>	0.6605	0.1500	0.6190	0.8181	0.3782	0.7462
<i>Min-k%</i>	0.7570	0.2081	0.6894	0.9154	0.5643	0.8400
<i>Min-k%++</i>	0.6353	0.1170	0.5003	0.7809	0.2849	0.5000
<i>Rényi</i>	0.6777	0.1649	0.6277	0.8330	0.3997	0.7528
<i>ICAS(ours)</i>	0.9942	0.9801	0.9658	0.9998	1.0000	0.9967

Table 8: Experiment results in PAR models.

Method	PAR-XL			PAR-XXL			PAR-3B		
	\uparrow AUROC	\uparrow TPR@5%	\uparrow ASR	\uparrow AUROC	\uparrow TPR@5%	\uparrow ASR	\uparrow AUROC	\uparrow TPR@5%	\uparrow ASR
<i>Loss</i>	0.5330	0.0662	0.5263	0.5904	0.1021	0.5689	0.7345	0.2299	0.6799
<i>Min-k%</i>	0.5370	0.0590	0.5263	0.5997	0.0829	0.5766	0.7478	0.2204	0.6932
<i>Min-k%++</i>	0.5275	0.0561	0.5198	0.5941	0.0782	0.5665	0.7566	0.2288	0.5056
<i>Rényi</i>	0.5389	0.0622	0.5287	0.5927	0.0828	0.5689	0.7327	0.2052	0.6775
<i>ICAS(ours)</i>	0.6519	0.1680	0.6086	0.7913	0.3682	0.7184	0.9616	0.8147	0.8952

Table 9: Experiment results in NAR models (Part 1).

Method	NAR-B			NAR-M		
	\uparrow AUROC	\uparrow TPR@5%	\uparrow ASR	\uparrow AUROC	\uparrow TPR@5%	\uparrow ASR
<i>Loss</i>	0.5055	0.0520	0.5016	0.5099	0.0528	0.5087
<i>Min-k%</i>	0.5058	0.0532	0.5046	0.5109	0.0548	0.5078
<i>Min-k%++</i>	0.5045	0.0536	0.5041	0.5061	0.0554	0.5053
<i>Rényi</i>	0.5317	0.0606	0.5210	0.5267	0.0619	0.5193
<i>ICAS(ours)</i>	0.5315	0.060	0.5210	0.5556	0.0705	0.5386

D Limitations

Our method relies on autoregressive generative models that support both conditional and unconditional prediction. As a result, it is not compatible with earlier autoregressive image generation models, such as VQVAE [36] and VQGAN [8], which only support conditional prediction.

E Future Work

A promising direction for future research is the extension of our approach to more fine-grained generative paradigms. For example, models like ControlVAR [20] and EditAR [23] leverage images as conditioning inputs, rather than class labels or textual descriptions. Exploring methods to simulate the unconditional generation

Table 10: Experiment results in NAR models (Part 2).

Method	NAR-L			NAR-XXL		
	\uparrow AUROC	\uparrow TPR@5%	\uparrow ASR	\uparrow AUROC	\uparrow TPR@5%	\uparrow ASR
<i>Loss</i>	0.5128	0.0542	0.5064	0.5501	0.0729	0.5359
<i>Min-k%</i>	0.5166	0.0578	0.5089	0.5637	0.0701	0.5442
<i>Min-k%++</i>	0.5103	0.0552	0.5100	0.5320	0.0575	0.5238
<i>Rényi</i>	0.5268	0.0627	0.5162	0.5463	0.0715	0.5332
<i>ICAS(ours)</i>	0.5768	0.0806	0.5532	0.7241	0.2000	0.6632

Table 11: Experiment results in LlamaGen models (Part 1).

Method	LlamaGen-B			LlamaGen-L			LlamaGen-XL		
	\uparrow AUROC	\uparrow TPR@5%	\uparrow ASR	\uparrow AUROC	\uparrow TPR@5%	\uparrow ASR	\uparrow AUROC	\uparrow TPR@5%	\uparrow ASR
<i>Loss</i>	0.5047	0.0521	0.5060	0.5170	0.0537	0.5133	0.5404	0.0625	0.5290
<i>Min-k%</i>	0.5211	0.0579	0.5105	0.5420	0.0651	0.5303	0.5804	0.0814	0.5560
<i>Min-k%++</i>	0.5151	0.0564	0.5135	0.5375	0.0652	0.5272	0.5729	0.0826	0.5560
<i>Rényi</i>	0.5019	0.0475	0.5028	0.5136	0.0498	0.5103	0.5339	0.0595	0.5255
<i>ICAS(ours)</i>	0.5438	0.0629	0.5323	0.5990	0.0946	0.5698	0.7119	0.1859	0.6529

Table 12: Experiment results in LlamaGen models (Part 2).

Method	LlamaGen-XXL			LlamaGen-3B		
	\uparrow AUROC	\uparrow TPR@5%	\uparrow ASR	\uparrow AUROC	\uparrow TPR@5%	\uparrow ASR
<i>Loss</i>	0.5810	0.0806	0.5599	0.7126	0.2054	0.6590
<i>Min-k%</i>	0.6446	0.1178	0.6046	0.8361	0.3049	0.7603
<i>Min-k%++</i>	0.6193	0.1067	0.5890	0.7426	0.1979	0.6870
<i>Rényi</i>	0.5689	0.0801	0.5497	0.6736	0.1800	0.6313
<i>ICAS(ours)</i>	0.8578	0.4372	0.7772	0.9855	0.9317	0.9409

Table 13: Experiment results in LlamaGen-CCA models (Part 1).

Method	LlamaGen-CCA-B			LlamaGen-CCA-L			LlamaGen-CCA-XL		
	\uparrow AUROC	\uparrow TPR@5%	\uparrow ASR	\uparrow AUROC	\uparrow TPR@5%	\uparrow ASR	\uparrow AUROC	\uparrow TPR@5%	\uparrow ASR
<i>Loss</i>	0.5090	0.0550	0.5076	0.5212	0.0578	0.5153	0.5513	0.0730	0.5348
<i>Min-k%</i>	0.5255	0.0593	0.5171	0.5503	0.0671	0.5360	0.6038	0.0878	0.5756
<i>Min-k%++</i>	0.5187	0.0574	0.5133	0.5457	0.0675	0.5353	0.6011	0.0976	0.5770
<i>Rényi</i>	0.5047	0.0521	0.5038	0.5164	0.0532	0.5126	0.5406	0.0653	0.5261
<i>ICAS(ours)</i>	0.5267	0.0624	0.5198	0.5627	0.0835	0.5459	0.6274	0.1425	0.5931

probability could also prove to be a valuable avenue for further investigation.

Additionally, autoregressive generation has been expanded to other modalities, such as video [13] and audio [24]. Assessing the

applicability of our approach to these modalities will be an important direction for future work.

Received 20 February 2007; revised 12 March 2009; accepted 5 June 2009

Table 14: Experiment results in LlamaGen-CCA models (Part 2).

Method	LlamaGen-CCA-XXL			LlamaGen-CCA-3B		
	↑ AUROC	↑ TPR@5%	↑ ASR	↑ AUROC	↑ TPR@5%	↑ ASR
<i>Loss</i>	0.6087	0.1097	0.5778	0.8338	0.4999	0.7606
<i>Min-k%</i>	0.7008	0.1443	0.6483	0.9533	0.6764	0.9044
<i>Min-k%++</i>	0.6958	0.1704	0.6455	0.9397	0.7697	0.8849
<i>Rényi</i>	0.5867	0.0969	0.5624	0.7598	0.3588	0.7013
<i>ICAS(ours)</i>	0.7412	0.2826	0.6791	0.9766	0.8827	0.9219